Available online at www.sciencedirect.com
ScienceDirect
Journal of Power Sources 172 (2007) 613–622
JOURNAL OF POWER SOURCES
www.elsevier.com/locate/jpowsour

Improvement of proton exchange membrane fuel cell electrical performance by optimization of operating parameters and electrodes preparation

A.J.-J. Kadjo [a], P. Brault [b], A. Caillard [b], C. Coutanceau [c], J.-P. Garnier [a], S. Martemianov [a,*]

[a] *Laboratoire d'Etudes Thermiques, UMR6608, ESIP-Université de Poitiers, CNRS, Poitiers F-86022, France*
[b] *Groupe de Recherche sur l'Energétique des Milieux Ionisés, UMR6606 Université d'Orléans, CNRS Polytech'Orléans BP6744, F-45067 Orléans Cedex 2, France*
[c] *Laboratoire de Catalyse en Chimie Organique, UMR6503 Université de Poitiers, CNRS, Poitiers F-86022, France*

Received 6 March 2007; received in revised form 9 May 2007; accepted 13 May 2007
Available online 18 May 2007

Abstract

The effect of operating parameters (cell temperature, humidifiers temperature, gases flows and pressures) on the performance of a 25 cm^2 surface area fuel cell is performed. After optimization, a homemade MEA fitted with electrodes prepared via the colloidal route leads to achieve reproducibly maximum power densities higher than 1.2 $W\,cm^{-2}$ with a total catalyst loading of 0.7 $mg_{Pt}\,cm^{-2}$ (corresponding to 1.7 $kW\,g_{Pt}^{-1}$). This electrical performance is higher to that obtained with a commercial MEA provided by fuel cell store (total platinum loading of 1.2 $mg\,cm^{-2}$ and power density close to 1 $W\,cm^{-2}$, corresponding to 0.75 $kW\,g_{Pt}^{-1}$). Based on this experience, two different homemade MEAs are tested under optimal operating conditions and compared to the commercial one. The final goal is to decrease significantly the platinum loading preserving at least equivalent PEMFC electrical performance. The method of catalyst deposition by plasma sputtering is used to further decrease the total catalyst loading down to 0.45 $mg_{Pt}\,cm^{-2}$. Very interesting performances (close to 0.7 $W\,cm^{-2}$) were obtained with this low-platinum loading MEA (corresponding to 1.6 $kW\,g_{Pt}^{-1}$). However, it was shown that the decrease of the platinum loading in the cathode from 0.35 to 0.1 $mg\,cm^{-2}$ affects the kinetics of oxygen reduction (exchange current density j_0 and Tafel slope b) and the resistance of the cell R, and hence the cell electrical performance.

Keywords: Optimization; Working conditions; Plasma sputtering; Platinum colloid; PEMFC; Electrical performance

1. Introduction

Over the past two decades, fuel cell technologies were extensively studied because they represent one of the most promising ways of energy production for transportation (propulsion and/or auxiliary power units) [1,2], nomad devices (mobile phones, computer, emergency) [3,4] or stationary systems [5,6]. Indeed, fuel cells convert directly and continuously the fuel (hydrogen) chemical energy into electric power, heat and water [7,8], without limitations due to the Carnot theorem and polluting evolutions.

PEMFC (proton exchange membrane fuel cells) using solid polymer membranes and working at low temperatures ($\leq$100 °C) are the subject of priority research in many countries. These studies are focused on the development of fuel cells and stacks with acceptable electrical performances for practical applications, price and lifetime. One of the challenges in its commercialization is the optimization of MEA electrical performance by adjusting the operating conditions, which can help to reduce the platinum loading in the electrodes and further to decrease the total cost of the fuel cells.

The electrical performance of fuel cells is known to be influenced by different operating conditions such as cell temperature, anode and cathode pressure and humidification of the reactant gases. Wang et al. [9] studied experimentally the effects of different operating parameters on the performance of PEMFC using pure hydrogen on the anode side and air on the cathode side.

* Corresponding author. Tel.: +33 5 49 45 39 04; fax: +33 49 45 35 39.
E-mail address: serguei.martemianov@univ-poitiers.fr (S. Martemianov).

0378-7753/$ – see front matter © 2007 Elsevier B.V. All rights reserved.
doi:10.1016/j.jpowsour.2007.05.019

Nomenclature

b	Tafel slope (mV decade^{-1})
E_{cell}	cell voltage (V)
E_{ideal}	ideal cell voltage (V)
E_r	reversible cell voltage (V)
$f_{H_2,c}$	flow of consumed hydrogen (mL mn^{-1})
$f_{H_2,t}$	total flow of hydrogen (mL mn^{-1})
F	Faraday constant (96,490 C mol^{-1})
ΔG_r	free Gibbs energy for the reaction of combustion of hydrogen in oxygen (-237 kJ mol^{-1} under standard conditions for the formation of liquid water)
ΔH_r	enthalpy of the reaction of combustion of hydrogen in oxygen (-286 kJ mol^{-1} under standard conditions for the formation of liquid water)
j	current density (mA cm^{-2})
j_0	exchange current density (mA cm^{-2})
n	number of electrons
P_a	anode backpressure (bar)
P_c	cathode backpressure (bar)
P_{H_2}	hydrogen partial pressure (bar)
P_{H_2O}	water partial pressure (bar)
P_{O_2}	oxygen partial pressure (bar)
P^0	reference pressure (1 bar)
R	perfect gas constant (8.31433 J K^{-1} mol^{-1})
S	active surface area of the MEA (25 cm^2)
R_{cell}	total cell resistance (Ω cm^2)
T_{cell}	cell working temperature (°C)
T_{huma}	temperature of the anode humidifier (°C)
T_{humc}	temperature of the cathode humidifier (°C)
V_m	molar volume of hydrogen (L mol^{-1})

Greek letters

η_E	potential efficiency
η_f	faradaic efficiency
η_r	reversible efficiency
ν_{H_2}	hydrogen stoichiometric factor

Freng et al. [10] have investigated analytically and experimentally the performance of PEMFC. Their model has focused on the cathode compartment of PEMFC. Hwang and Hwang [11] provided a parametric study of a double-cell stack of PEMFC. Huyn and Kim [12] studied experimentally the effect of external humidity on fuel cell performance. Mugikura and Asano [13] have compared the performance of several types of fuel cells. Kazim et al. [14] investigated the influence of cathode operating conditions on the performance of PEMFC using a mathematical model. This non-exhaustive list of works dealing with the influence on the operating conditions indicates the great importance of this aspect for optimizing the PEMFCs performance.

One of the major targets for PEMFC large-scale development is their high cost. The platinum-based catalysts represent a non-negligible part of the total cost of the fuel cell. Typically, PEMFC electrodes are loaded with 0.3–0.5 mg cm^{-2} leading to electrical performances in the range of 0.7–0.8 W cm^{-2} (i.e. close to 1 kW g^{-1} of Pt), which represents a platinum cost close to 45$ kW^{-1} (considering a cost of 45$ g^{-1} of platinum). Therefore, the development of researches leading in the same time to the increase of the electrical performances of PEMFCs and to the decrease the platinum loading of MEA (membrane electrode assembly) is of great interest. In this paper, two ways have been run to reach this objective: the optimization of the operating parameters (temperature, humidification of reactants and pressure) and the improvement of MEAs fabrication technology, notably the electrodes preparation by either colloidal or plasma sputtering route. The optimization of the operating parameters led to a systematic investigation of the parameters that affect the PEMFC performance and further to a better understanding of the effects of these parameters. The development of physical methods for the fabrication of low platinum loading electrodes, as for example plasma sputtering methods, well controlled by the industry in the field of microelectronics, could give great scientific and industrial benefits.

2. Experimental

2.1.1. Fuel cell test station

Experimental studies of fuel cell performances need appropriated apparatus. In the present study fuel cell test station (FCTS) manufactured by Fuel Cell Technologies, Inc. is used. The overview of the test station is shown on Fig. 1a. This test station allows controlling the cell temperature, humidification temperatures, backpressures and mass flow rates on both the anode and the cathode sides. A principle schema of the FCTS is shown in Fig. 1b. Fuel cell temperatures and humidification temperatures are controlled by a microprocessor-based temperature/process controller CN76122 T/C. Reactant gases are humidified by passing through external water tanks. Regulation of the water temperature in the humidifiers allows controlling gas humidification. Two backpressure regulators at the outlets of the fuel cell are used to control the operating pressure. The station includes also a computer-based control and data acquisition system based on Labview^{TM} software. The computer system is connected to mass flow controllers, which are located before the humidifier. The mass flow rate is set and read through the software. Polarization curves are recorded at constant mass flow rates of reactant gases in the inlet of the cell. The polarization curves are obtained by controlling the HP6050 Electronic Load, which measures the cell output voltage and current. In this study, pure hydrogen and oxygen are used as fuel and oxidant, respectively.

2.1.2. Assembling of fuel cells

Assembling of cells is a delicate procedure, which has a very important influence on the cell performance. Fig. 2 shows the main elements of a single PEMFC and its overview before and after assembling.

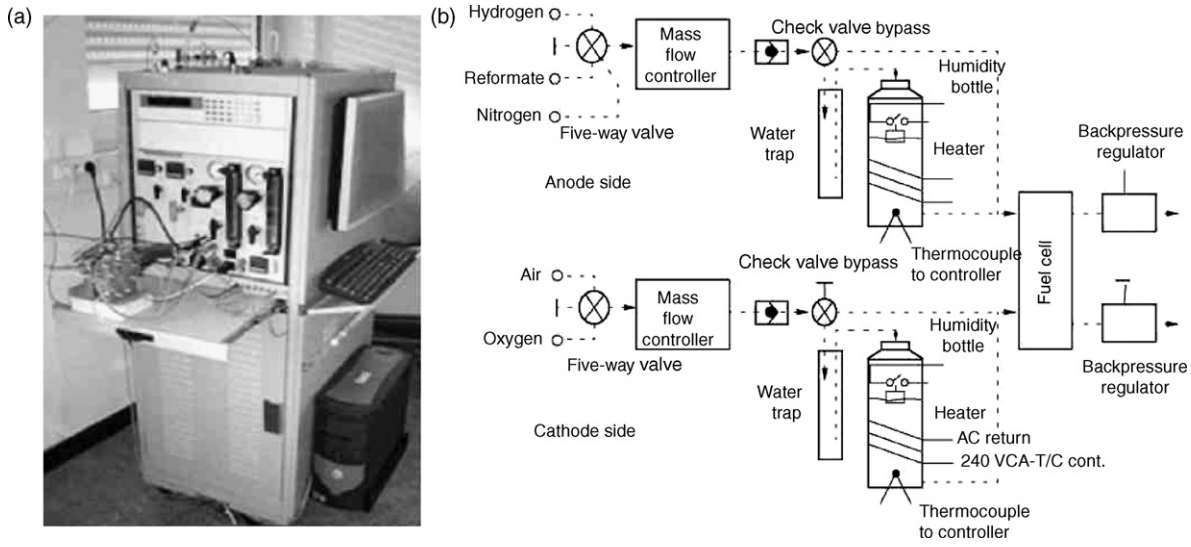

Fig. 1. (a) Photograph of the fuel cell test station and (b) schematic representation of experimental apparatus.

Special attention has been paid for the correct assembling of fuel cells, in particular, for the choice of the bolts torque that clamp the fuel cell together. The importance of this factor has been discussed by Lee et al. [15]. A correct choice of the bolts torque (8 Nm) allows obtaining well reproducible results for each type of MEA used in our experiments as it was showed in previous works [16,17]. The experiments have been carried out with a single PEM fuel cell (surface area of 5 cm × 5 cm).

Four different types of MEA have been tested. As a reference, we used a commercial MEA purchased at Fuel Cell Store (US) composed with a Nafion® 112 membrane, anode and cathode with platinum loadings of 0.2 and 1 mg cm^{-2}, respectively (MEA 2). Gas diffusion layer based on carbon cloth was used in the commercial MEA. Three homemade types of MEA were also tested; the methods of their fabrication are described below.

2.1.3. MEA fabrication

The 25 cm^2 surface area MEAs are prepared by hot pressing the homemade electrodes at 130 °C for 90 s under a pressure of 35 kg cm^{-2}, on a pre-treated Nafion® 112 membrane. MEA 1 type is composed of symmetric electrodes (0.35 mg_{Pt} cm^{-2}, a Pt 40 wt.%/C), MEA 2 type is composed of a 0.1 mg_{Pt} cm^{-2} sputtered platinum anode and a 0.35 mg_{Pt} cm^{-2} chemical cathode and MEA 3 type is composed of a 0.35 mg_{Pt} cm^{-2} chemical anode and a 0.1 mg_{Pt} cm^{-2} sputtered platinum cathode.

2.1.4. Synthesis of Pt/C catalysts by colloidal route and electrode preparation

Colloidal precursors are synthesized according to the procedure described by Bönnemann et al. [18], but slightly modified. All experiments are carried out under argon, using anhydrous salts and dry solvents. Reducing agent $N^+(C_nH_{2n+1})4[BEt_3H]^-$ is prepared by mixing stoichiometric amounts of tetraalkylamonium bromide $[N^+(C_nH_{2n+1})_4Br^-]$ and potassium triethylborohydride $[K(BEt_3H)]$ in tetrahydrofuran (THF). While added to this solution, the metallic salts ($PtCl_2$ from Alfa Aesar) are reduced according to the following reaction:

$$PtCl_2 + 2N^+(C_nH_{2n+1})4[BEt_3H]^- \rightarrow Pt[N^+(C_nH_{2n+1})_4 Cl^-]_2 + 2BEt_3 + H_2 \quad (1)$$

The colloidal precursors are dispersed onto a high specific area carbon substrate (Vulcan XC72). The carbon supported

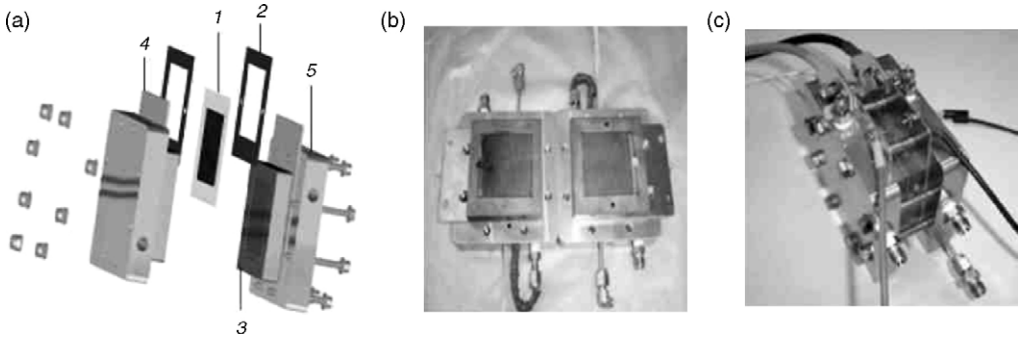

Fig. 2. (a) Schematic representation, of the single fuel cell assembling: (1) MEA, (2) gaskets, (3) bipolar plates, (4) current collectors and (5) end plates. (b) Photograph of the disassembled 25 cm^2 surface area single fuel cell. (c) Photograph of the assembled 25 cm^2 surface area single fuel cell.

metal powder is obtained after thermal treatment of the precursor at 300 °C under air for 1 h. The platinum particles are found to have a mean diameter close to 2.7 nm which is in agreement with previous results [19,20].

Homemade electrodes are prepared from ink composed of a Nafion® solution (5 wt.% from Aldrich), the desired amount of catalytic powder and water as solvent, brushed on a carbon diffusion layer (DL). DL is homemade using a carbon cloth from Electrochem Inc. on which was brushed ink made of Vulcan XC72 carbon powder and PTFE dissolved in isopropanol. The gas diffusion electrodes are loaded with 3.5 mg cm^{-2} of a mixture of carbon powder and 30 wt.% PTFE. The metal loading of chemical electrodes is close to 0.35 mg_{Pt} cm^{-2}, with a Pt 40 wt.%/C catalyst and a 40 wt.% Nafion®/platinum ratios.

2.1.5. Platinum plasma sputtering

Platinum is deposited by plasma sputtering on the same DL than above. The low-pressure plasma set-up is described in Fig. 3. More details are given in previous works [21,22]. To proceed the sputtering, the platinum target faced the DL in a vacuum reactor. −300 V negatively biased target is sputtered by energetic argon ions of inductive plasma created by using an external planar antenna (also known as TCP antenna). This excitation antenna is powered by a 13.56 MHz RF generator coupled to a tunable matching box. All electrodes were prepared with the same Ar working pressure (0.5 Pa), target–substrate distance (5.5 cm) and input power (200 W). The sputtering time is adjusted to obtain a Pt loading of 0.1 mg cm^{-2}. Plasma electrodes display the following characteristics—C: 3.5 mg cm^{-2}; PTFE: 1 mg cm^{-2}; Nafion®: 0.3 mg cm^{-2}; Pt: 0.1 mg cm^{-2}. Previous scanning electron microscopy analysis showed that each carbon particles are covered by Pt nano-clusters forming a relatively dense clustering film on the DL surface.

3. Results analysis

The effect of different operating parameters on the fuel cell behavior is studied from several series of measurements: cell temperature, humidification temperature of gases and back-pressure of reactants. Inside each series of measurements, the recorded $E(j)$ cell voltage versus current density curves are treated using the method developed by Ticianelli et al. [23] and Hirano et al. [24] to draw some kinetic data. The following equations were used:

$$E = E_0 - b \log j - R_{\text{cell}} j \tag{2}$$

$$E_0 = E_r + b \log j_0 \tag{3}$$

where j is the current density at the potential E, E_r the reversible potential of the cell, j_0 and b the exchange current density and Tafel slope for orr, respectively, and R_{cell} is the total resistance causing the linear variation in the cell potential versus current density (j). The electric data up to the end of the linear region of the $E(j)$ curves were analyzed, for which the square of the correlation coefficient r^2 was always taken higher than 0.995.

This treatment was possible assuming that mass transport limitations and activation overpotentials at the hydrogen electrode are negligible, and accepting that the reactants act as ideal gases (their activity equals their partial pressure) and that the activity of water is 1. Then, the open circuit voltage can be expressed as follows:

$$E_r = -\frac{\Delta G_r(T)}{2F} + \frac{RT}{2F} \ln\left(\frac{P_{H_2}(P_{O_2})^{1/2}}{P_{H_2O}} \frac{1}{(P^0)^{1/2}}\right) \tag{4}$$

where $\Delta G_r(T)$ is the free Gibbs energy, R the perfect gas constant (8.31433 J (K mol)$^{-1}$), T the cell temperature, F the Faraday constant (96,490 C mol^{-1}) and P^0 is the reference pressure (atmospheric pressure).

Each experiment was repeated three times in order to verify the repeatability of the measurements. The statistical calculations lead to standard deviations on the current density, which vary with the cell current density from 5 to 40 mA cm^{-2}, i.e. a maximum relative uncertainty lower than 5% (2 s).

The cell efficiency with respect to hydrogen consumption was calculated under optimized experimental conditions for the different tested MEAs at a cell voltage of 0.65 V. First the stoichiometric factor ν_{H_2} was estimated as follows:

$$\nu_{H_2} = \frac{\text{total flow of hydrogen}}{\text{consumed flow of hydrogen}} = \frac{f_{H_2,t}}{f_{H_2,c}} \tag{5}$$

where $f_{H_2,c}$ and $f_{H_2,t}$ are the hydrogen consumed and total flows, respectively:

$$f_{H_2,c} = \frac{SV_m}{nF} j \tag{6}$$

with S the active surface area of the MEA and V_m the molar volume of hydrogen. Then the cell efficiency can be expressed as follows:

$$\eta_{\text{cell}} = \eta_r \eta_f \eta_E \frac{1}{\nu_{H_2}} \tag{7}$$

$$\eta_{\text{cell}} = \frac{nFE_r}{-\Delta H_r} \frac{E(j)}{E_r} \eta_f \frac{1}{\nu_{H_2}} \tag{8}$$

$$\eta_{\text{cell}} = -\frac{nF}{\Delta H_r} E(j) \eta_f \frac{1}{\nu_{H_2}} \tag{9}$$

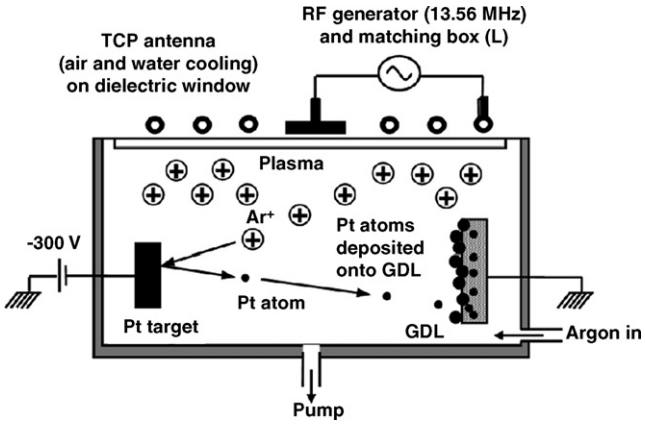

Fig. 3. Schematic of the plasma sputtering reactor.

where η_r is the reversible efficiency, η_f the faradaic one, η_E the potential one [25] and ΔH_r is the enthalpy of the reaction of hydrogen combustion in oxygen. In Eq. (7), the expression $-\Delta H_r/nF$ is comparable to an ideal cell voltage, which should correspond to the production of electricity without heat evolution. The cell efficiency can then be expressed as follows:

$$\eta_{cell} = \frac{E(j)}{E_{ideal}} \frac{1}{\nu_{H_2}} \eta_f \quad (10)$$

In this equation, E_{ideal} can take two different values depending on the formation of either gaseous or liquid water. Under the pressure and temperature operating conditions used in the present work, the formation of liquid water can be assumed. Then, the value of E_{ideal} should take a value corresponding to the superior calorific power, i.e. $286 \times 10^3/2 \times 96490 = 1.48$ V, assuming that the value of ΔH_r is constant over the cell temperature range used in this work. A faradaic efficiency $\eta_f = (n_{exp}/n_{th}) = 1$ is also assumed, i.e. that the reduction reaction of oxygen is complete, occurring via a four-electron process to form water (no production of hydrogen peroxide).

4. Result and discussion

4.1. Optimization of operating parameters on a commercial MEA

The first series of measurements concerns the influence of the fuel cell temperature on the electrical performances under humidified inlet gases conditions. Fig. 4 shows polarization curves cell temperatures in the range from 40 to 80 °C. In all cases the humidification temperatures are 5 °C lower than that of the cell. Anode and cathode backpressures are set to 2 bar. An increase in the fuel cell voltage for a given current density with the temperature is viewed in this figure, particularly in the high current densities region. In other words, the performance of the fuel cell is improved with increasing the cell operating temperature under humidified gases conditions. Table 1 gives the values of E_0, b, R_{cell} and j_0. Although no significant effect is visible in the kinetic region of the polarization curves (i.e. in the low current density region), the improvement of the fuel cell performance has to be related with the increase of the oxygen kinetics (increase of the Tafel slope from 0.65 to 0.72 mV decade^{-1} and of j_0 by one order of magnitude with the increase of the temperature from 40 to 80 °C). In addition, the decrease of the overall resistance of the system (from 0.20 to 0.13 Ω cm^2) has likely a more pronounced effect in the high current density region, due to both higher ion conductivity in the Nafion® membrane and lower mass transport resistance for higher temperatures.

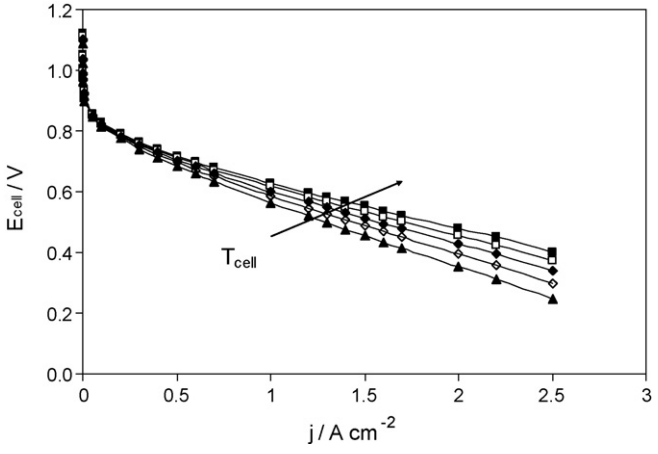

Fig. 4. Cell voltage E_{cell} vs. current density j obtained with a homemade MEA (anode and cathode loadings: 0.35 mg_{Pt} cm^{-2}, membrane Nafion® 112) for different operating temperatures. The gases are humidified by passing through bottles containing water maintained at a temperature 5 °C lower than the cell temperature. 0.6 L_{H_2} min^{-1}, 0.4 L_{O_2} min^{-1} and $P_a = P_c = 2$ bar. (▲) $T_{cell} = 40$ °C; (◇) $T_{cell} = 50$ °C; (♦) $T_{cell} = 60$ °C; (□) $T_{cell} = 70$ °C; (■) $T_{cell} = 80$ °C.

Table 1
Electrode kinetic parameters for oxygen reduction drawn from $E(j)$ curves of Fig. 4

T_{cell} (°C)	E_0 (V)	E_r (V)	b (V decade^{-1})	R_{cell} (Ω cm^2)	j_0 ($\times 10^7$ A cm^{-2})
40	0.767	1.229	0.065	0.199	0.73
50	0.769	1.221	0.066	0.183	1.32
60	0.768	1.214	0.068	0.165	2.58
70	0.765	1.206	0.070	0.146	5.17
80	0.765	1.198	0.072	0.133	9.67

The effects of humidification of inlet gases on the fuel cell performance are studied in a second and third series of experiments (Fig. 5a and b). In these experiments the cell temperature is kept at 80 °C and backpressures are set to 2.5 bar; anode and cathode flow rates are set to 0.5 L_{H_2} min^{-1} and 0.35 L_{O_2} min^{-1}, respectively. In Fig. 5a, which illustrates the effect of anode humidification (T_{huma}), the cathode humidifier temperature remaining constant ($T_{humc} = 40$ °C), one can see an increase in the cell voltage with the increase of the anode humidification at a given current density. Moreover, the slope of the linear part of the polarization curve (which is mainly related to the resistive limitation of the cell) is influenced by T_{huma}. This again indicates that the increase of anode humidification leads to the decrease of the electrical resistance of the membrane, and hence to the enhancement of the cell performance. This is confirmed by the calculation of E_0, b, R_{cell} and j_0 as given in Table 2. It appears than the values of E_0, b and j_0 do not change significantly, whereas the resistance R decreases with the increase of T_{huma}. This indicates that the water transport through the membrane does not balance the evaporation of water by temperature and hydrogen flow. This leads to the drying of the membrane in the anode side and to the limitation in proton conductivity. Fig. 5b shows the influence of the cathode humidifier temperature, T_{humc}; in these experiments the anode humidifier temperature is kept constant (T_{huma} = 75 °C) and the other operating parameters are the same as in the previous experiments. The performance of the fuel cell decreases with the increase of the cathode humidifier temperature. The same effect was pointed out by Wang et al. [9]. These authors attributed this phenomenon to the decrease of the effective porosity of the gas diffusion layers by the flooding of the electrode and further to the decrease of the reactant concentration in the catalytic layer. The calculation of E_0, b, R_{cell} and j_0 (Table 2) indicates that conversely to that is observed at the cathode side, the increase of oxygen humidification seems to enhance the kinetics of oxygen reduc-

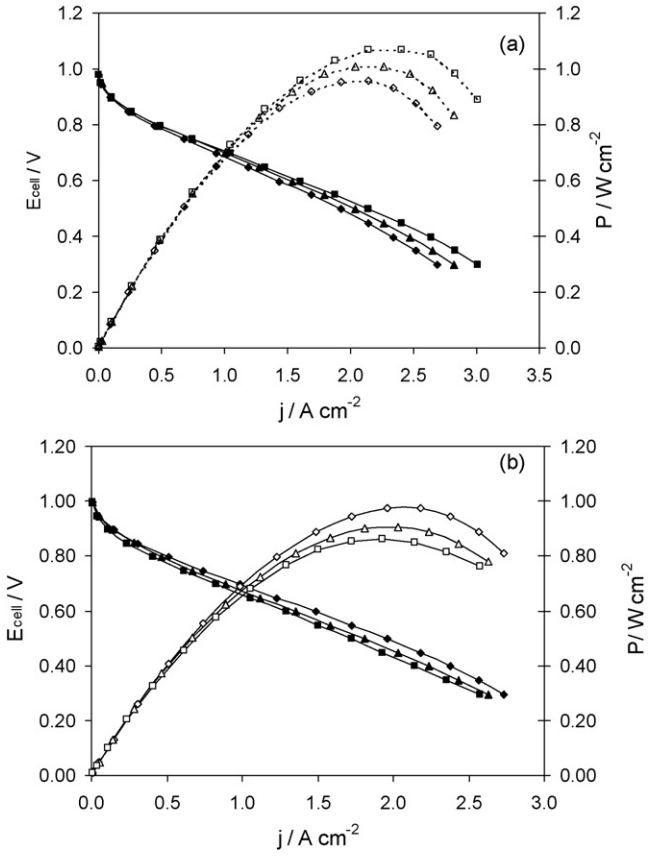

Fig. 5. Cell voltage E_{cell} and power density P vs. current density j curves recorded at 80 °C (anode and cathode loadings: 0.35 $mg_{Pt}\,cm^{-2}$, membrane Nafion® 112): a) for different anode humidifier temperatures T_{huma} with a cathode humidifier temperature, T_{humc}, set to 40 °C. 0.5 $L_{H_2}\,min^{-1}$, 0.35 $L_{O_2}\,min^{-1}$ and $P_a = P_c = 2.5$ bar. (♦, ◊) $T_{huma} = 70$ °C; (▲, △) $T_{huma} = 75$ °C; (■, □) $T_{huma} = 80$ °C; (b) for different cathode humidifier temperatures, T_{humc} with an anode humidifier temperature, T_{huma}, set to 75 °C. 0.5 $L_{H_2}\,min^{-1}$, 0.35 $L_{O_2}\,min^{-1}$ and $P_a = P_c = 2.5$ bar. (♦, ◊) $T_{humc} = 40$ °C; (▲, △) $T_{humc} = 50$ °C; (■, □) $T_{humc} = 70$ °C.

tion (the value of b and j_0 tends to increase with the increase of T_{humc}), but in the same time the resistance increases too. This latter effect is in agreement with the flooding of the electrode, notably in the high current density region where the formation of water at the cathode is important, which leads to increase the electrode flooding and to decrease the accessibility of oxygen to the catalyst sites. As a consequence, the cell voltage decreases more drastically with the current density.

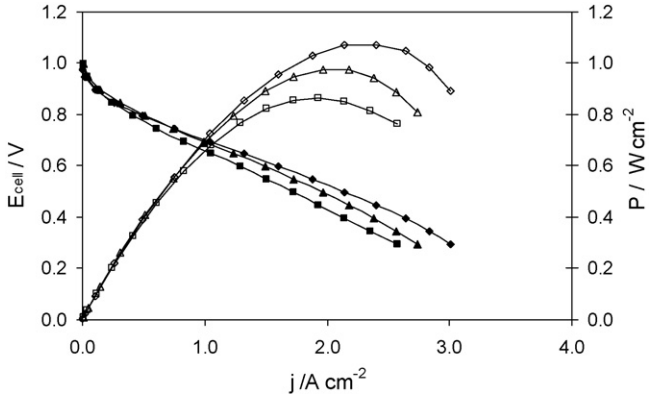

Fig. 6. Cell voltage E_{cell} and power density P vs. current density j curves recorded at 80 °C for different operating pressures on the anode and cathode sides. $T_{humc} = 40$ °C, $T_{huma} = 75$ °C, 0.5 $L_{H_2}\,min^{-1}$, 0.35 $L_{O_2}\,min^{-1}$. (■, □) $P_a = P_c = 1$ bar; (▲, △) $P_a = P_c = 2$ bar; (♦, ◊) $P_a = P_c = 2.5$ bar.

At last, the effect of fuel cell pressure on PEM fuel cell performance is studied in a fourth series of experiments (Fig. 6). In these experiments the operating pressures in the anode and in the cathode sides of fuel cell are equilibrated and are varied in the range from 1 to 2.5 bar. The operating temperature of the cell is fixed at 80 °C. Humidified hydrogen and oxygen are used ($T_{huma} = 75$ °C; $T_{humc} = 40$ °C). The increase of the back-pressure of the inlet gases enhances the cell performance. According to result presented in Table 3, the increase of the pressure seems to have a significant effect only on the cell resistance. The improvement of the cell performance due to the increase of the operating pressures can be explained by the increase of the diffusivity of the reactant gases, or to the decrease of the pressure drop between the inlet and the outlet of the cell (due to the reactants consumption) with the increase of the operating pressure. Amirinejad et al. [26] observed that the pressurization of the cathode side involves more important effect on the cell performance than pressurization of the anode side. However, in our experiments, the drilling of the MEA has occurred several times when pressures in the anode and cathode sides were not equilibrated. Therefore, we did not succeed to optimize the pressure differential between the anode and the cathode for the improvement of fuel cell performance, because of the lifetime limitation.

Although optimization of the operating parameters of PEMFCs has been extensively discussed in numerous papers

Table 2
Electrode kinetic parameters for oxygen reduction drawn from $E(j)$ curves of Fig. 5a and b

T_{huma} (°C)	E_0 (V)	E_r (V)	b (V decade^{-1})	R_{cell} (Ω cm^2)	j_0 ($\times 10^7$ A cm^{-2})
70	0.864	1.203	0.049	0.184	1.26
75	0.865	1.203	0.050	0.169	1.81
80	0.861	1.203	0.051	0.159	1.95
T_{humc} (°C)	E_0 (V)	E_r (V)	b (V decade^{-1})	R_{cell} (Ω cm^2)	j_0 ($\times 10^6$ A cm^{-2})
40	0.877	1.203	0.058	0.185	2.37
50	0.876	1.203	0.060	0.204	3.41
70	0.862	1.203	0.064	0.207	4.65

Table 3
Electrode kinetic parameters for oxygen reduction drawn from $E(j)$ curves of Fig. 6

P reactants (bar)	E_0 (V)	E_r (V)	b (V decade^{-1})	R_{cell} (Ω cm^2)	j_0 ($\times 10^7$ A cm^{-2})
1	0.874	1.182	0.043	0.216	0.64
2	0.895	1.198	0.046	0.203	2.83
2.5	0.866	1.203	0.048	0.164	1.29

[9–12,27–29], it still remains an open question. If some points seem clear enough, as for example the increase of the cell performance with the increase of the cell temperature, the influence of some other parameters is not completely identified. For example, in agreement with Wang et al. [9] we showed that the performance of a fuel cell decreases with the increase of the cathode humidifier temperature, in contrary to that was proposed by Amirinejad et al. [26]. A lot of results concerning performances of single PEMFC can be found in the literature, but operating conditions are often very different [30–32 and references therein]. Then, standardization of fuel cell experiments in order to facilitate the comparison between laboratories is very important. But, this is not the goal of this paper. However, the best performances presented by some authors were extracted from some recently published papers [9,26,30,31] in order to make some comparisons with our results. Table 4 summarizes the best operating conditions proposed by these authors and related maximum power density. Usually the most successful tests are provided at cell temperatures around 80°. Fig. 7 shows the reproducible and stable cell performance achieved with our homemade MEA after optimization of the operating parameters and fuel cell assembly procedure, i.e. high cell temperature (85 °C), low T_{humc} (35 °C), high T_{huma} (80 °C) and high reactant pressures ($P_a = P_c = 3$ bar). The electrical performance exceeds 1 W cm^{-2}, which is the performance level generally required as a target for mobile applications of PEMFC technologies. The control of the parameters to reach such a result allowed us working on the optimization of new technology of MEA fabrication, in particular with respect to the decrease of platinum loading in the electrodes. This aspect is another key point for the large-scale development of PEMFC technology. Some of the obtained results are presented in the next paragraph.

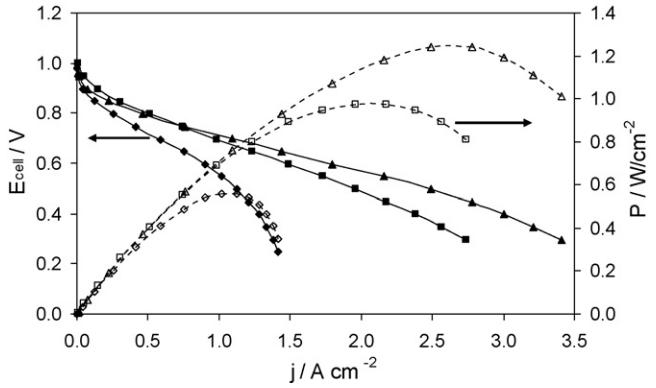

Fig. 7. Comparison of the fuel cell performance obtained with different MEAs. (♦, ◊) MEA 1: homemade electrode via the colloidal route before assembling procedure optimization; (■, □) MEA 1 bis: homemade electrode via the colloidal route after assembling procedure optimization; anode and cathode loadings: 0.35 mg$_{Pt}$ cm^{-2}; (▲, △) MEA 2: commercial MEA after assembling procedure optimization; anode loading: 0.2 mg$_{Pt}$ cm^{-2}, and cathode loading: 0.35 mg$_{Pt}$ cm^{-2}. Fuel cell operating conditions: $T_{cell} = 85$ °C, $T_{humc} = 35$ °C, $T_{huma} = 80$ °C, 0.6 L$_{H_2}$ min^{-1}, 0.4 L$_{O_2}$ min^{-1} and $P_c = 3$ bar.

Lifetime is another target for PEM fuel cell applications. Fig. 8 presents the voltage E_{cell} versus time recorded at $j = 0.96$ A cm^{-2} (for which the stability is also showed), under optimized operating conditions. The cell displays a very good stability in electrical performance for more than hundred hours, the cell voltage remaining constant (0.7 V). It has to be noted that this result was obtained thanks to some improvements of the assembling technology [16,17]. First tests realized without improvement led to a lifetime of a few hours. The principal cause of this short lifetime was the drilling of MEAs.

4.2. Effect of MEA fabrication

Fuel cells are non-linear systems. Then, extrapolation of the results obtained at a given scale of operating conditions to another one is a delicate problem. For this reason fuel cell experiments realized with different MEAs were compared at the optimal operating conditions previously determined, keeping into account 1 W cm^{-2} as one of the important targets. The operating conditions retained for this study are: $T_{cell} = 85$ °C, $T_{huma} = 80$ °C, $T_{humc} = 35$ °C, 0.6 L$_{H_2}$ min^{-1}, 0.4 L$_{O_2}$ min^{-1} and $P_a = P_c = 3$ bar. Some information concern-

Table 4
Operating conditions used by different authors to obtained the best fuel cell performance

Membrane	Wang et al. [3], Nafion® 115 (125 μm)	Williams et al. [21], Nafion® (25–50 μm)	Amirinejad et al. [18], Nafion® 117 (175 μm)	Wee et al. [22], Nafion® 112 (50 μm)
Platinum loading (mg cm^{-2})	0.4	0.56–0.57	0.4	0.1
Pt loading anode (mg cm^{-2})	0.4	0.56–0.57[a]	0.4	0.1
Cell surface area (cm^2)	7.2 × 7.2	5	5	–
T_{cell} (°C)	70	70	80	80
T_{huma} (°C)	70	70	80	80
T_{humc} (°C)	70	70	80	80
P_a (bar)	3	1	2	2.6
P_c (bar)	3	1	2	2.7
P_{max} (W cm^{-2})	0.74	0.45	0.22	0.71

[a] PtRu anode.

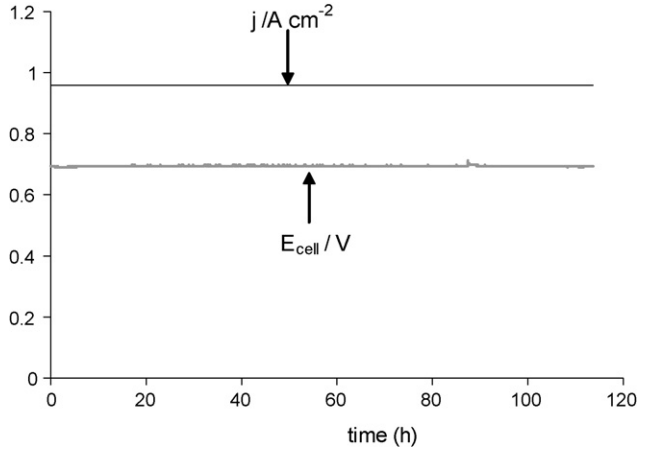

Fig. 8. Voltage and current density curves vs. time, recorded in a 25 cm^2 single fuel cell at a fixed current density of 0.96 A cm^{-2}. Fuel cell operating conditions: $T_{cell} = 85\,^{\circ}C$, $T_{humc} = 35\,^{\circ}C$, $T_{huma} = 80\,^{\circ}C$, 0.6 L_{H_2} min^{-1}, 0.4 L_{O_2} min^{-1} and $P_c = 3$ bar.

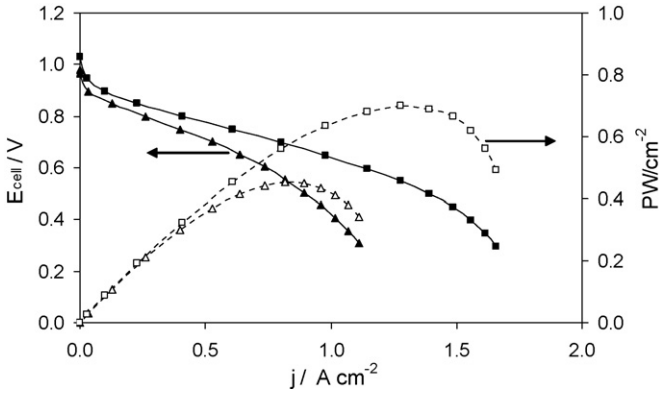

Fig. 9. Voltage and Power density curves vs. current density for two homemade MEAs with different catalysts loading in the anode and cathode. (■, □) Anode prepared by plasma sputtering and cathode prepared via the colloidal route; platinum loadings are 0.1 and 0.35 mg_{Pt} cm^{-2}, respectively; (▲, △) anode prepared via the colloidal route and cathode prepared by plasma sputtering; loadings are 0.35 and 0.1 mg_{Pt} cm^{-2}, respectively. Fuel cell operating conditions: $T_{cell} = 85\,^{\circ}C$, $T_{humc} = 35\,^{\circ}C$, $T_{huma} = 80\,^{\circ}C$, 0.6 L_{H_2} min^{-1}, 0.4 L_{O_2} min^{-1}, $P_a = P_c = 3$ bar.

ing optimization of fuel cell assembling can be found elsewhere [16,17].

First, the benefic effect of the cell assembling procedure [16,17] is confirmed in Fig. 7 with MEA 1 and MEA 1 bis. The catalysts used in these assemblies are synthesized via the colloidal method [18–20]. The electrodes (platinum loading of 0.35 mg_{Pt} cm^{-2} in both electrodes) are pressed against a Nafion® 112 membrane. The MEA 1 was tested before the development of the procedure of cell assembling [16,17], whereas optimized cell assembling procedure was used before testing MEAs 1 bis and 2. The commercial MEA 2 was provided by fuel cell store (platinum loadings of 0.2 and 1 mg_{Pt} cm^{-2} in the anode and cathode, respectively; Nafion® 112). The correct assembling of fuel cell allows reaching considerable improvement (approximately 60%) for the maximum fuel cell performance, which increases from 0.5 W cm^{-2} to almost 1.3 W cm^{-2}. Second, the homemade MEA allows, in spite of the lowest platinum loading (0.7 mg_{Pt} cm^{-2} against 1.2 mg_{Pt} cm^{-2} for the commercial MEA), to obtain a maximum higher power density (approximately 30%) than that obtained with the commercial MEA (1.0 W cm^{-2}). The cell efficiency at 0.65 V has increased from 11% (MEA 1) to 21% (MEA 1 bis) with the optimization of working parameters, and from 17.5% to 21% between the FCS MEA 2 and homemade MEA 1 bis. The kinetics parameters are given in Table 5. The exchange current density is higher with the commercial MEA than with the homemade one, which can rather be related to the lower platinum loading in electrodes than to the lower activity of the catalyst as indicates by the higher Tafel slope obtained with the homemade MEA. However, the more important contribution in the enhancement of the cell performance is certainly the decrease of the MEA resistance (0.19 and 0.12 Ω cm^2, for the commercial and homemade MEAs, respectively), i.e. to the enhancement in the reactant diffusion and/or in the electrode/membrane resistance interfaces. Therefore, the homemade MEA displays higher electrode kinetics, which is related to the catalyst activity and lower resistance which is related to the MEA fabrication technology (structure of the gas diffusion layer and active layer, membrane/electrode interface and Nafion® 112 pretreatment).

Platinum deposition using plasma sputtering technique [21–33] can be a good alternative to prepare low-platinum MEAs. Two MEAs are prepared with different catalyst loadings (anode 0.1 mg_{Pt} cm^{-2} and cathode 0.35 mg_{Pt} cm^{-2} in MEA 3; anode 0.35 mg_{Pt} cm^{-2} and cathode 0.1 mg_{Pt} cm^{-2} in MEA 4). In these MEAs, the low platinum loading electrodes (0.1 mg_{Pt} cm^{-2}) are prepared by plasma sputtering, whereas the higher-loading electrode (0.35 mg_{Pt} cm^{-2}) are chemically prepared via the colloidal route. Fig. 9 shows the polarization and power density curves obtained with both MEAs. Two important remarks can be drawn from these curves. The first one is that the worst cell performance is achieved when the low-platinum loading electrode is used as cathode. The maximum achieved power density is 0.45 W cm^{-2} against 0.7 W cm^{-2} when the platinum loading in the cathode is of 0.35 mg_{Pt} cm^{-2}. The decrease of catalyst loading in the cathode has much more important negative effect on the cell performance in comparison with the decrease of platinum loading in the anode. Second, although the total platinum loading is about three times lower than that in the commercial FCS assembly, the maximum achieved power density is

Table 5
Kinetics data obtained drawn from Figs. 7 and 8 with different homemade MEAs

Assembly	E_0 (V)	E_r (V)	b (V $decade^{-1}$)	R_{cell} (Ω cm^2)	j_0 ($\times 10^7$ A cm^{-2})
MEA 1 bis	0.836	1.203	0.060	0.125	7.29
MEA 2	0.885	1.203	0.051	0.192	5.43
MEA 3	0.867	1.203	0.054	0.239	7.81
MEA 4	0.873	1.203	0.025	0.321	5.22×10^{-7}

MEA 1 (anode and cathode: 0.35 mg_{Pt} cm^{-2}, Nafion® 112), MEA 2 (commercial MEA from FCS, anode 0.2 mg_{Pt} cm^{-2}, cathode 1.0 mg_{Pt} cm^{-2}), MEA 3 (cathode 0.35 mg_{Pt} cm^{-2}, anode 0.1 mg_{Pt} cm^{-2}, Nafion® 112) and MEA 4 (anode 0.35 mg_{Pt} cm^{-2}, cathode 0.1 mg_{Pt} cm^{-2}, Nafion® 112). Cell operating conditions: $T_{cell} = 85\,^{\circ}C$, $T_{huma} = 80\,^{\circ}C$, $T_{humc} = 35\,^{\circ}C$, 0.6 L_{H_2} min^{-1}, 0.4 L_{O_2} min^{-1} and $P_a = P_c = 3$ bar.

only 30% lower, which confirms that the plasma-assisted catalyst fabrication is a convenient alternative to chemical synthesis for fuel cell electrode fabrication, in terms of cell performance, cost and industrial control of the technic (which is used in large scale in the field of thin film fabrication for microelectonic devices application).

But, the first remark indicates clearly that the oxygen reduction reaction at the cathode is the limiting step. Results of the modelisation derived from the method of Ticianelli et al. [23] and Hirano et al. [24] are given in Table 5. First, the values of Tafel slope and the exchange current density obtained with the MEA 3 (cathode loaded with 0.35 $mg_{Pt}\,cm^{-2}$) is of the same order than that obtained with MEA 1 bis and 2, which indicates that the decrease of the platinum loading in the anode does not affect the kinetics. But, comparing MEA 3 and 4, the Tafel slope decreases with the decrease of the cathode platinum loading, from 0.054 down to 0.025 mV $decade^{-1}$. This can be related to the decrease of the intrinsic activity of the catalyst, i.e. oxygen reduction kinetics. The kinetics limitation is confirmed by the values of the exchange current density j_0 which undergoes a drastic decrease when the platinum loading in the cathode is decreased from 0.35 to 0.1 $mg_{Pt}\,cm^{-2}$ ($j_0 = 7.38 \times 10^{-7}$ and 5.2×10^{-14} A cm^{-2}, respectively). Previous study at platinum particles dispersed in a polyaniline film pointed out the kinetics limitation of highly dispersed platinum particles on the electrocatalytic reduction of dioxygen [33]. This fact involves a decrease in the fuel cell efficiency from 14% and 9% for the MEA 3 and 4 respectively. But, these values of the cell efficiency are lower than that obtained with MEA 1 bis and MEA 2, which also indicates a limitation in the hydrogen oxidation due to lower platinum loading. Moreover, one can see that MEAs with sputtered electrodes display higher resistance and that sputtered cathode leads to higher resistance limitation than sputtered anode, 0.32 and 0.24 $\Omega\,cm^2$, respectively. The increase of the cell resistance can likely be related to the decrease of the density of platinum active sites in this thin catalyst layer, which is more drastic for oxygen reduction reaction than for hydrogen oxidation reaction.

Moreover, it was shown that structure of the deposition of platinum by plasma sputtering on porous carbon diffusion layer leads to nanoparticles with a mean apparent size close to 3.0 nm, which agglomerate in clusters of 8–10 nm even for low platinum loading [34]. For metal loadings higher than 20 $\mu g_{Pt}\,cm^{-2}$, a thin platinum film surrounding carbon particles is formed. This platinum thin film, which is formed on the top surface of the carbon DL, may have a more important role on the activity of oxygen reduction, which is known to be structure dependent, than on hydrogen oxidation. Then, plasma sputtering conditions have to be ameliorated to improve the platinum deposition and electroactivity towards hydrogen oxidation and oxygen reduction, as well as the formulation of the electrode (weight ratios of Pt/C, Pt/Nafion, etc.). Moreover, for oxygen reduction, more studies have to be done to determine the minimum platinum loading convenient for reaching an acceptable cell performance of at least 1 W cm^{-2}. However, the structure of the deposition by plasma sputtering and the low platinum loading in the electrodes has certainly an important effect on durability. In the time scale of the experiments (1 day), the assemblies with low platinum loading based-electrodes (prepared via the plasma sputtering route) displayed good stability, but further long-term duration tests (as for chemically prepared electrodes) have to be made. The preliminary results presented in this paper are very encouraging for the development of low-platinum loading electrode fabricated by plasma sputtering.

5. Conclusion

Optimization of operating parameters in fuel cell experiments and the technology of fuel cell assembly made possible to reach reproducible electrical performance higher than 1 W cm^{-2} with homemade MEAs. Based on this experience, three different homemade MEAs were tested under optimal operating conditions, with as final goal a significant decreasing of the platinum loading for at least equivalent PEMFC electrical performance. The MEA fabricated with electrode prepared via the colloidal route made possible to obtain maximum power density higher than 1.2 W cm^{-2} with total catalyst loading of 0.7 $mg_{Pt}\,cm^{-2}$ corresponding to 1.7 W mg_{Pt}^{-1}, which is more than two times higher than that is obtained with a commercial MEA from FCS (0.9 W cm^{-2} with total platinum loading of 1.2 $mg_{Pt}\,cm^{-2}$, corresponding to 0.75 W mg_{Pt}^{-1}). The method of catalyst deposition by plasma sputtering was also used to further decreasing of the total catalyst load down to 0.45 $mg_{Pt}\,cm^{-2}$. Very interesting performances (close to 0.7 W cm^{-2}) were obtained with this low-platinum loading MEA. This performance corresponds in term of platinum utilization efficiency close to 1.6 W mg_{Pt}^{-1}, which is two times higher than that obtained with commercial MEA. But, considering that plasma sputtering is a clean and well-controlled process by microelectronic manufacturers, it could be a good way for fuel cell electrodes or/and MEAs fabrication. Moreover, the powerful method of plasma sputtering let foresee the possibility of optimization of the platinum deposition (structure of the platinum thin film, particle size, depth profile, etc.) to improve cell performance.

Acknowledgements

The authors acknowledge the CNRS "Programme Energie" and "Actions Concertées Incitatives" for financial support. The experiments presented in this paper used the resources of the "ICOGEPAC" technological and research platform (Engineering of the components and technical Management of Fuel Cells).

References

[1] R. Nolte, J. Power Sources 4573 (2001) 1.
[2] M. Wang, J. Power Sources 112 (2002) 307.
[3] D. Chu, R. Jiang, K. Gardner, R. Jacobs, J. Schmidt, T. Quakenbush, J. Stephens, J. Power Sources 96 (2001) 174.
[4] A. Heinzel, C. Hebling, M. Müller, M. Zedda, C. Müller, J. Power Sources 105 (2002) 250.
[5] G.J.K. Acres, J. Power Sources 100 (2001) 60.
[6] J. Hamelin, K. Agbossou, A. Laperrière, F. Laurencelle, T.K. Bose, Int. J. Hydrogen Energy 26 (2001) 625.

[7] J.-F. Fauvarque, Piles à combustible et leurs applications, Ann. Chim. Sci. Mater. 26 (2001) 1.
[8] M. Prigent, Les piles à combustible: état du développement et des recherches en cours à l'aube de l'an 2000, Institut Français du Pétrole Rueil Malmaison (France), 1997.
[9] L. Wang, A. Husar, T. Zhou, H. Liu, Int. J. Hydrogen energy 28 (2003) 1263–1272.
[10] Y.M. Ferng, Y.C. Tzang, B.S. Pei, C.C. Sun, A. Su, Int. J. Hydrogen Energy 29 (2004) 381.
[11] J.-J. Hwang, H.-S. Hwang, J. Power Sources 104 (2002) 24.
[12] D. Hyun, J. Kim, J. Power Sources 126 (2004) 98.
[13] Y. Mugikura, K. Asano, Electr. Eng. Jpn. 138 (2002) 24.
[14] A. Kazim, P. Forges, H.T. Liu, Int. J. Energy Res. 27 (2003) 401.
[15] W.-K. Lee, C.-H. Ho, J.W.V. Zee, M. Murthy, J. Power Sources 84 (1999) 45.
[16] J.-J.A. Kadjo, J.-P. Garnier, S. Martemianov, J.-P. Maye, C. Coutanceau, S. Grigoriev, Proceedings of the French Heat Transfer Congress Transfers in Heterogeneous Mediums, Peninsula of Giens, 2004, pp. 928–932.
[17] J.-J.A. Kadjo, J.-P. Garnier, J.-P. Maye, F. Relot, S. Martemianov, Russian J. Electrochem. 42 (2006) 467.
[18] H. Bönnemann, W. Brijoux, R. Brinkmann, R. Fretzen, T. Joussen, R. Köppler, B. Korall, P. Neiteler, J. Richter, J. Mol. Catal. 86 (1994) 129.
[19] L. Dubau, F. Hahn, C. Coutanceau, J.-M. Léger, C. Lamy, J. Electroanal. Chem. 554/555 (2003) 407.
[20] L. Demarconnay, C. Coutanceau, J.-M. Léger, Electrochem. Acta 49 (2004) 4513.
[21] P. Brault, A. Caillard, A.L. Thomann, J. Mathias, C. Charles, R.W. Boswell, S. Escribano, J. Durand, T. Sauvage, J. Phys. D: Appl. Phys. 37 (2004) 3419.
[22] A. Caillard, P. Brault, J. Mathias, C. Charles, B.W. Boswell, T. Sauvage, Surf. Coat. Technol. 200 (2005) 391.
[23] E.A. Ticianelli, C.R. Derouin, A. Redondo, S. Srinivasan, J. Electrochem. Soc. 185 (1988) 2209.
[24] S. Hirano, J. Kim, S. Srinivasan, Electrochim. Acta 42 (1997) 1587.
[25] F. Vigier, S. Rousseau, C. Coutanceau, J.-M. Léger, C. Lamy, Topics Catal. 40 (2006) 111.
[26] M. Amirinejad, S. Rowshanzamir, M.H. Eikani, J. Power Sources 161 (2006) 872.
[27] F. Barbir, PEM Fuel Cells: Theory and Practice, Elsevier Academic Press (Eds.).
[28] V. Mishra, F. Yang, R. Pitchumani, J. Power Sources 141 (2005) 47.
[29] G.H. Guvelioglu, H. Stenger, J. Power Sources 163 (2007) 882.
[30] M.V. Williams, H.R. Kunz, J.M. Fenton, J. Power Sources 135 (2004) 122.
[31] J.H. Wee, K.-Y. Lee, S.H. Kim, J. Power sources 165 (2007) 667.
[32] H.A. Gasteiger, S.S. Kocha, B. Sompalli, F.T. Wagner, Appl. Catal. B: Environ. 56 (2005) 9.
[33] A. Caillard, C. Coutanceau, P. Brault, J. Mathias, J.-M. Léger, J. Power Sources 162 (2006) 66.
[34] C. Coutanceau, M.-J. Croissant, T. Napporn, C. Lamy, Electrochim. Acta 46 (2000) 579.